JOURNAL OF SPACECRAFT AND ROCKETS
Vol. 38, No. 2, March–April 2001

Investigation of Remote Antenna Assembly for Radio Communication with Reentry Vehicle

I. F. Belov,* V. Ya. Borovoy,* V. A. Gorelov,† A. Y. Kireev,‡ A. S. Korolev,* and E. A. Stepanov‡
Central Aerohydrodynamic Institute, 140180, Moscow Region, Russia

Consideration is given to the experimental investigation of the original method of providing radio communications with a reentry vehicle along the trajectory section when a vehicle is surrounded by plasma of the ionized shock layer. The method suggests placing of the antennas in special small containers. The containers are located at about zero angle of attack on a pylon ahead of the bow shock wave generated near a vehicle. Because of the small container bluntness low level of ionization near the antennas could be provided. But many problems connected with heating and thermal protection of the container and pylon arise in this case. Therefore along with the measurements of ionization near the container, heating and thermal protection of the container and pylon and their influence on the vehicle aerodynamics were investigated. The experiments were performed in four hypersonic wind tunnels of different types in Mach-number range from 6.5 to 20.5. Various measurement methods were used. The investigation shows that the remote antenna assembly can provide uninterrupted radio communication with the reentry vehicle.

Nomenclature

C_i	=	rolling-moment coefficient
C_L	=	lifting coefficient
C_m	=	pitching-moment coefficient
C_n	=	yawing-moment coefficient
d	=	diameter of remote antenna assembly container, 0.08 m
F	=	model planform area
G	=	total mass-flow rate of injected gas
H	=	flight altitude
i	=	gas enthalpy
K	=	correlation parameter for nonequilibrium ionization
L	=	model length
M	=	Mach number
m	=	local mass-flow rate of injected gas, $\rho_w v_w$
n	=	concentration of particles
P	=	pressure
q	=	heat flux
R	=	nose bluntness radius
Re_0	=	Reynolds number for stagnation temperature viscosity, $\rho_\infty V_\infty R/\mu_0$
$Re_{\infty L}$	=	Reynolds number for undisturbed flow viscosity, $\rho_\infty V_\infty L/\mu_\infty$
S	=	distance from stagnation point along surface
T	=	temperature
t	=	time
V	=	flow velocity, flight velocity
v_w	=	injection velocity
X_{cg}, Y_{cg}	=	center-of-mass position coordinate
y	=	shock-layer coordinate normal to the surface
α	=	angle of attack
β	=	sideslip angle
Λ	=	nonequilibrium ionization parameter
ρ	=	density
Ψ	=	dihedral angle of wing
$\Delta\Psi$	=	angle of wing deflection
ω	=	radio signal frequency
ω_p	=	plasma frequency

Subscripts

e	=	electron
eq	=	equilibrium
i	=	ionization, ions
j	=	injected gas
max	=	maximum
t	=	total
w	=	wall conditions
0	=	stagnation point
1	=	for unit Reynolds number
∞	=	freestream

Superscripts

L/D	=	lift/drag
R/L	=	right/left

I. Introduction

RADIO communication during the vehicle reentry in the Earth's atmosphere is a vital challenge posed by the practice of space flights. Radio communication is known to be affected by plasma formations that occurred near the vehicle at high flight velocities. Interaction of electromagnatic waves and plasma layer can result to communication blackout between the vehicle and relevant tracking stations.

Several methods can be used to eliminate the plasma shielding and thus to provide radio communication with the vehicle. First of all, a frequency band proper for radio communication must be chosen. But achievable frequency bands are usually limited by the technical possibilities of radio facilities. Radio communication can be improved if the antennas are located in zones with minimum electron concentration. Particularly for vehicles flying at large angles of attack, there is a rationale to place the antennas in the separation zone on the lee side of the vehicle and use a satellite for retranslating. But at smaller angles of attack (i.e., at higher lift/drag ratios) and at maneuvers, the conditions for radio communications through a satellite can become worse. In the 1970s the possibilities of active impact on the ionization level were investigated with the help of injection electrophilic liquids or gases into the shock layer[1] and creation of magnetic field in the ionized layer surrounding the antenna.[2] Use of these methods meets significant difficulties when applied to a hypersonic large vehicle having large-scale nose bluntness radius because of the large thickness of the ionized layer. Another approach to the

Presented as Paper 99-3739 at the 30th Plasmadynamics and Lasers Conference, Norfolk, VA, 28 June–1 July 1999; received 30 September 1999; revision received 30 November 2000; accepted for publication 5 December 2000.

*Head of Branch, Hypersonic Division, Zhukovsky-3.
†Deputy Head of Division, Hypersonic Division, Zhukovsky-3. Member AIAA.
‡Leading Scientist, Hypersonic Division, Zhukovsky-3.

Table 1 Used regimes of wind tunnels

Wind tunnel	Type	Diameter[a] (square)[b] of jet cross section, m (m^2)	Mach number, M	Unit Reynolds number Re_∞, m^{-1}	Total pressure P_t, bar	Total temperature T_t, K	Test duration, s
IT-2	Hot shot	0.53[a]	19.6	1.4×10^6	740	2400	0.1
			17.9	5.7×10^6	930	1600	0.1
			20.5	1.5×10^5	250	6500	0.1
T-116	With resistance heater	1×1[b]	3.0–9.7	$10.2–5.7 \times 10^6$	1.1–80	300–1100	350
T-117	With arc heater	1.0[a]	18.7	0.3×10^5	150	3000	60
			14	0.1×10^6	100	2000	
T-122	With arc heater	0.13[a]	6.5	1×10^5	5	5000	1800

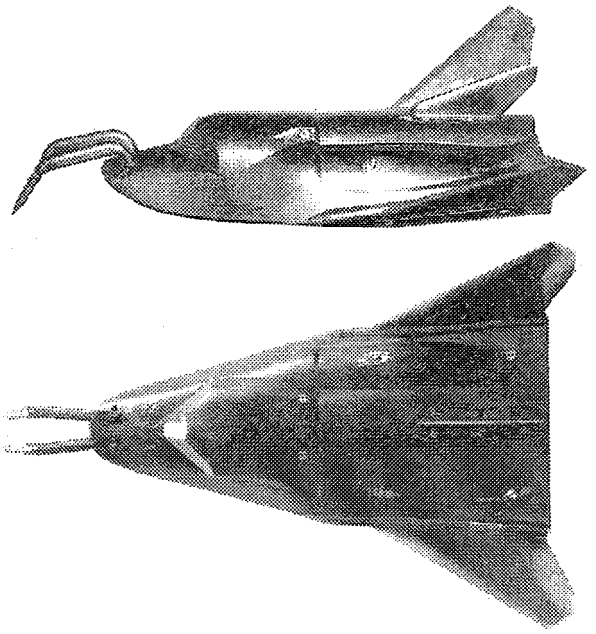

Fig. 1 Photograph of the vehicle model with RAA.

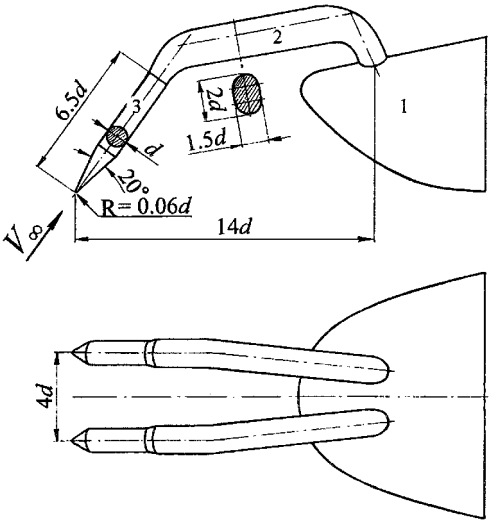

Fig. 2 Scheme of RAA configuration on the vehicle model nose part: 1, vehicle model nose part; 2, RAA pylon; and 3, antenna container.

problem of radio communication is investigated here. It is based on application of remote antenna assemblies (RAA) mounted at zero or small angle of attack on a pylon in the nose of fuselage (or on the wing ends). RAA presents itself as a cylinder containing antennas and having a conical nose. The antennas are placed ahead the bow shock of the vehicle, i.e., outside the thick shock layer created by the vehicle. Of course, the container generates a shock wave, too, and the antennas are streamlined by plasma. Nevertheless, if the bluntness radius and angle of attack of the container are small, the ionization level around the container can be low enough to provide direct radio communication between the vehicle and ground stations in centimeter and decimeter ranges of wavelengths without the help of satellite retranslate. The described method of radio communication with a hypersonic vehicle with the help of RAA was suggested in the USSR in the 1970s by Yu. Khodotaev, expert of the Aerospace Corporation "Energia." RAA was supposed to be used on the vehicle "Buran." The main idea and the design solutions should be tested on the large flying model "Bor.[3]" Two RAA should be symmetrically mounted in the nose of Bor as shown in Figs. 1 and 2. In connection with development of RAA for the vehicle Bor, extensive research was carried out in TsAGI. The following problems have been investigated: the possibility of achievement at an acceptable level of air ionization near the container; dependence ionization level on RAA dimensions and distributed gas injection intended for heat protection; influence of the RAA on the aerodynamic characteristis of the vehicle; peculiarities of aerodynamic heating of the pylon and container caused by interference of shock waves; the possibility to save the shape of the RAA nose by the help of distributed gas injection. The main results of these studies are presented in this paper.

The experimental investigations have been performed in TsAGI's four wind tunnels (see Table 1). All of the aerodynamic facilities just mentioned, except IT-2, present themselves blowdown wind tunnels with ejector exhaust. The IT-2 facility is a Hot Shot wind tunnel. Electrical discharge in its plenum chamber results in release energy accumulated in condenser battery. Additional characteristics of the facilities are presented in Ref. 4. The complex investigations performed demonstrate the possibility to solve all of the main problems associated with the creation of remote antennas assemblies providing radio communication with a vehicle throughout its flight trajectory.

II. Peculiarities of Ionization Process Near RAA

The ionization level near the antenna container depends to a great extent on the gas ionization intensity in the shock layer at the stagnation point near the RAA nose. With the small nose bluntness radius, viscous and nonequilibrium processes are of significant importance in the ionization. At the stagnation point the nonequilibrium ionization effect can be characterized by parameter $\Lambda_i = \tau_i / t_s \cong \tau_i \cdot V_\infty / R$, ($\tau_i$- is the characteristic ionization time behind the shock wave (see, e.g., Ref. 5; t_s is the gas flow time in the shock layer), while the viscosity effect can be characterized by the Reynolds number $Re_0 = V_\infty \rho_\infty R / \mu_0$. Reference 3 states that a maximum ionization level at the stagnation point for bodies with a spherical bluntness in a viscous shock layer depends on the correlation parameter $K = Re_0 \cdot \Lambda_i / (\Lambda_i^2 + 1)$, i.e., $n_{e0}/n_{e0\text{eq}} = f(K)$, where n_{e0} is the nonequilibrium electron concentration at the stagnation point and $n_{e0\text{eq}}$ is the equilibrium concentration. Figure 3 presents maximum values of n_{e0} at the stagnation point of RAA for the catalytic surface of the nose with bluntness radii of 5 and 20 mm for Buran and Bor reentry trajectories. The trajectory parameters V (at $V > 4$ km/s) and H are summarized in Table 2.

The results given in Fig. 3 are obtained using the correlation function $n_{e0}/n_{e0\text{eq}} = f(K)$. The symbols refer to check calculations of n_{e0} in numerical simulation based on the full Navier–Stokes equations (NEQNAST code[3]). When a RAA with a bluntness radius of $R = 5$ mm is used in the Buran vehicle, the values of n_{e0} can be four orders of magnitude smaller than equilibrium ionization levels $n_{e0\text{eq}}$.

Table 2 Buran and Bor reentry trajectories

	V, km/s	
H, km	Buran	Bor
80	7.2	7.3
70	6.6	7.2
60	5.0	6.8
55	4.2	6.2
50	—	4.0

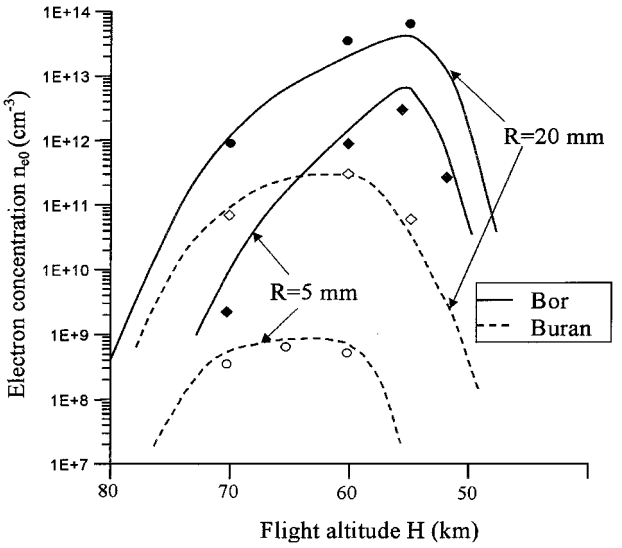

Fig. 3 n_{e0} as function of flight altitude for Buran and Bor vehicle trajectories.

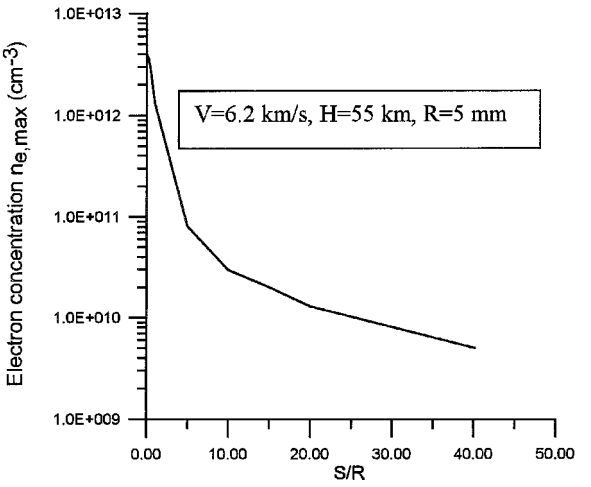

Fig. 4 Calculated $n_{e,\max}$ in a shock layer.

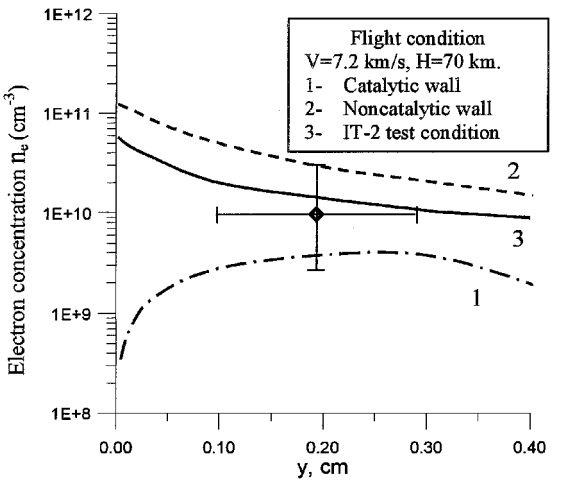

Fig. 5 Measured (♦) and calculated electron concentration vs coordinate y along stagnation line.

Even when $R = 20$ mm, a value of $n_{e0}/n_{e0\text{eq}}$ the order of 10^{-2} is predicted. As for Bor vehicle deceleration at lower altitudes, the application of the RAA is not so effective. But in this case the values of n_{e0} are also more than the order of magnitude smaller than respective equilibrium values at the stagnation point of the Bor vehicle nose when a maximum value of n_{e0} is attained at an altitude of the order of 55 km for $R = 5$ mm. Figure 4 demonstrates the NEQNAST-based calculations of maximum electron concentrations $n_{e\,\max}$ in a viscous shock layer along S of the RAA spherical-conical part for the Bor vehicle flight at 55 km. It is seen that $n_{e\,\max} \cong 10^9$ cm^{-3} at the antenna location on the RAA ($S/R > 40$). This makes it possible to realize radio communications through the RAA over centimetric and decimetric bands of electromagnetic waves. However, for real conditions of applying the RAA on the vehicles it is also necessary to consider the influence of distributed cold gas injection (air or nitrogen) into the nose (see Sec. IV.C), used to provide thermal protection of the nose with a small bluntness radius, on air ionization in the shock layer near the RAA. The intense injection results in an increased shock wave standoff distance from the RAA nose surface. The analysis of pictures showing flows over the RAA (see Sec. IV.C) has revealed that with the intense injection the shock wave curvature radius near the nose can be risen several times. To assess the injection effect on gas ionization near the RAA, some experimental investigations were carried in the IT-2 Hot-Shot wind tunnel. It is impossible to ensure full simulation of nonequilibrium ionization processes at hypersonic velocities in modern wind tunnels. Only approximate simulation problems can be considered for some flight conditions. In Ref. 3 the principles of approximate simulation of ionization processes near the RAA in the IT-2 wind tunnel are set forth for the case of a hypersonic viscous shock layer using the correlation parameter K. Model reproduction in the IT-2 wind tunnel of absolute values of n_{e0} in the viscous shock layer near the RAA demands satisfying the equalities $K = K'$ and $n_{e0\text{eq}} = n'_{e0\text{eq}}$ (the left-hand sides of the relations refer to full-scale conditions, whereas the right-hand sides with the superscript $'$ concern the laboratory conditions), which can be achieved for individual flight trajectory points only. In investigating the injection influence on ionization near the RAA, it became possible to accomplish simulation of n_{e0} at an altitude of 70 km for Buran flight trajectory ($V_\infty = 7.2$ km/s). This outcome is illustrated in Fig. 5, which presents the calculated distribution of n_e in the viscous shock layer at the stagnation point of the RAA with a bluntness radius of $R = 5$ mm. Curves 1 and 2 represent the distribution of n_e in flight conditions for catalytic and noncatalytic RAA nose surfaces, respectively, and curve 3 shows the calculation results for flows over the RAA model in the IT-2 wind tunnel ($T_t = 6500$ K, $P_t = 250$ atm, $M = 20.5$, noncatalytic model surface). Figure 5 also presents the value of n_{e0} measured using a wall electric probe installed at the stagnation point of a model made from an insulating material. The diameter of the probe placed flush with the model surface is 2 mm. This probe was used to measure the ion concentration at a distance equal to the probe layer thickness of 0.2 mm. The probe measurements were processed relying on the results of special methodical studies.[6] In general, our probe measurement method is similar to that used in Ref. 7. The measurement accuracy is shown in Fig. 5. Measured values of n_{e0} at the stagnation point of the model with a radius of 160 mm were of the order of 10^{13} cm^{-3}, while the electron concentration in gas flow at the IT-2 nozzle exit was "frozen" at the level of $n_{e\infty} \sim 10^8$ cm^{-3}. As a whole, the background gas flow ionization level in the IT-2 impeded the ionization simulation near the RAA because at $R = 5$ mm and $S/R > 1$ the calculated values of n_e under the simulation conditions are less than the concentration of $n_{e\infty}$ in the freestream flow. In view of this, the experimental investigations of the injection influence were of a qualitative nature. The main objective of these investigations is to show that in case of intense injection the electron concentration near the RAA at the antenna location does not exceed the critical level

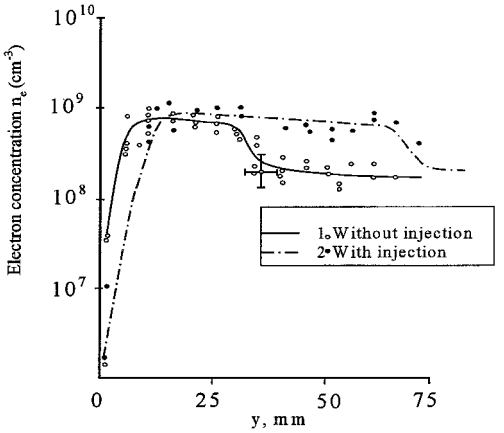

Fig. 6 Measured electron concentrations in shock layer near RAA model with and without cold gas injection vs coordinate y.

of the order of 10^9 cm^{-3}, which provides transmission of centimetric and decimetric electromagnetic waves through plasma near the RAA.

The experiments with injection were carried out in the IT-2 wind tunnel using a full-scale model. A nose from porous Ni-Cr alloy was installed in the model (see Sec. IV.C) to provide nitrogen injection at 290 K and 3 atm. In this case full-scale injection parameters were simulated: $P_{0j}/P_0' = 10^2$. A gas-distributing device for scheduled distribution of the injected gas mass flow along the nose generatrix was placed in the internal cavity of the porous nose.

The electron concentration distribution in the shock layer near the RAA was measured using a rake with cylindrical electric probes. Eight probes were placed at an equal distance of 5 mm from each other, the probe electrode diameter being 0.7 mm. Their end-face section was isolated by conical fairings. The probes were operated in the mode of collecting ion and electron current in the transition regime in terms of the Knudsen number. Preliminarily, peculiarities of the cylindrical probe operation in supersonic flows were studied in detail.[8] The probe rake was used to measure distributions of n_e in the shock layer in section $S/R = 50$ corresponding to the antenna location zone in the RAA. Figure 6 shows measured distributions of n_e near the RAA ($S/R = 50$) without nitrogen injection (points and curve 1) and with injection (points and curve 2). Injection results in a considerable increase in the plasma formation thickness near the RAA. Maximum values of n_e with injection slightly differ from respective values of n_e without injection not exceeding the level of the order of 10^9 cm^{-3}, which is critical for the RAA operation in conditions under study.

III. Influence of RAA on the Vehicle's Aerodynamic Characteristics

Various techniques of arranging the antenna container ahead of the bow shock wave front of a large-scale Bor-type vehicle in the lifting body configuration are studied.[3] The symmetric arrangement of two antenna containers on remote antenna assemblies placed in the body nose is an optimal variant for vehicles of such a type (Figs. 1 and 2). The aerodynamic configuration of this vehicle is chosen from the condition of providing its trimming at hypersonic velocities when angles of attack are high and close to critical values. Rotatable outboard wings and a small-area vertical tail are used as stabilizing surfaces on the vehicle. The chosen RAA arrangement variant is shown in Fig. 2. To provide self-trimming of the vehicle with the RAA at hypersonic velocities when $\alpha = 50$–55 deg is an important problem in developing radio communication through plasma. At these angles of attack, the RAA must be oriented in the flight velocity direction ($\alpha_{RAA} = 0$ deg.). It is also desirable that the aerodynamic characteristics of the vehicle with the RAA and without them be close to each other. The estimates reveal that the most complete solution of these problems for the vehicle under study can be obtained by choosing a relevant center-of-mass position, by arranging the outboard wings with the dihedral angle of $\Psi = 40$ deg, and by using additional gasdynamic control engines in the yaw channel. To verify experimentally the influence of the RAA on the vehicle's aerodynamic characteristics, a test series is carried out in the TsAGI T-116 wind tunnel[4] for the vehicle model with the RAA and without them. The vehicle model is tested at $\alpha = 30$–60 deg and $\beta = -4$–$+6$ deg. In this test series the experimental data are also obtained as concerns the effectiveness of differentially deflected wing outboards by angles $\Delta\Psi^{R/L} = \pm 5$ deg and $\Delta\Psi^{R/L} = \pm 10$ deg and the aerodynamic characteristics of the vehicle model with the RAA in some unscheduled situations.

The forces and moments acting on the vehicle model are measured by a six-component strain-gauge balance. In calculating the aerodynamic force coefficients, the body planform area $F = 0.07167$ m^2 is taken as a characteristic size, whereas the pitching-, rolling-, and yawing-moment coefficients are calculated for the same area, length $L = 0.4389$ m, and span $l = 0.2195$ m, respectively.

The pitching-, rolling-, and yawing-moment coefficients are calculated for a conditional center-of-mass position with the coordinates $X_{cg} = 0.56$ L (from the body nose); $Y_{cg} = 0.08$ L (from the central part of the lower body surface). According to the results of the statistical analysis of multiple tests, the errors $\bar{S}$ of aerodynamic characteristics of the vehicle model with the RAA over the test range of Mach numbers M_∞ and angles of attack do not exceed the following values:

$$\bar{S}c_D = \pm 0.00694 \qquad \bar{S}c_Y = \pm 0.00159$$

$$\bar{S}c_L = \pm 0.00505 \qquad \bar{S}c_n = \pm 0.000334$$

$$\bar{S}c_m = \pm 0.000769 \qquad \bar{S}c_l = \pm 0.000444$$

The investigations of the vehicle model's aerodynamic characteristics show that for $M_\infty = 3 \ldots 9.7$ and $Re_{\infty L} = (3.43 \ldots 2.5) \times 10^6$ the RAA arrangement does not exert any influence on the lifting properties; it causes a slight increase in the drag and pitch-up moment increments, which rise as the angle of attack increases. At $M_\infty > 7$ such variations in the moment characteristics at the start of pitching results in a favorable shift of the trim angle of attack toward greater values. As an example, Fig. 7 gives functions C_L, $L/D = f(\alpha)$, and $C_m = f(\alpha)$ at $M_\infty = 9.7$; $Re_{\infty L} = 2.5 \times 10^6$ for the vehicle model with the RAA and without them. It is seen that at this Mach number and a specified center-of-mass position the vehicle model is self-trimmed with the RAA at $\alpha = 52$ deg, while without the RAA at $\alpha = 44$ deg.

To provide self-trimming of the vehicle with the RAA at $\alpha = 55$ deg, the center of mass must slightly be shifted aft by 0.2% of the body length (Fig. 7). The use of the RAA on the vehicle model exerts a destabilizing effect basically on the directional static stability (Fig. 8). To provide the vehicle control in yaw and roll along the

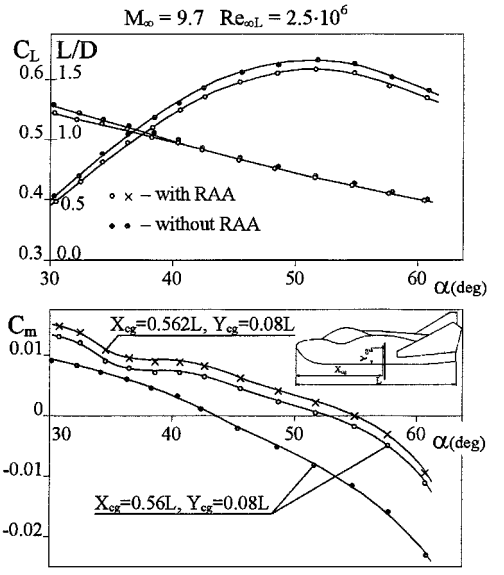

Fig. 7 Lifting coefficient, L/D ratio, and pitching-moment coefficient of the vehicle model with and without RAA vs angle of attack.

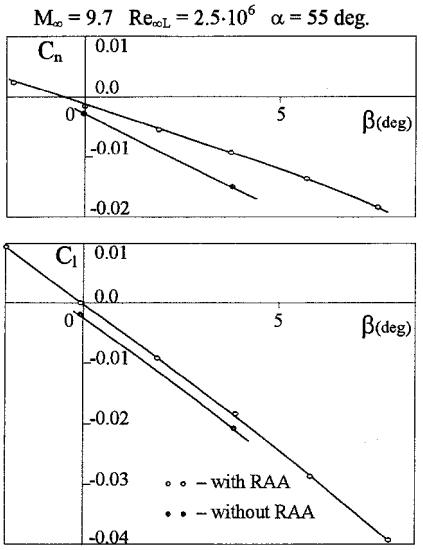

Fig. 8 Yawing- and rolling-moment coefficients of the vehicle model with and without RAA vs sideslip angle at angle of attack 55 deg.

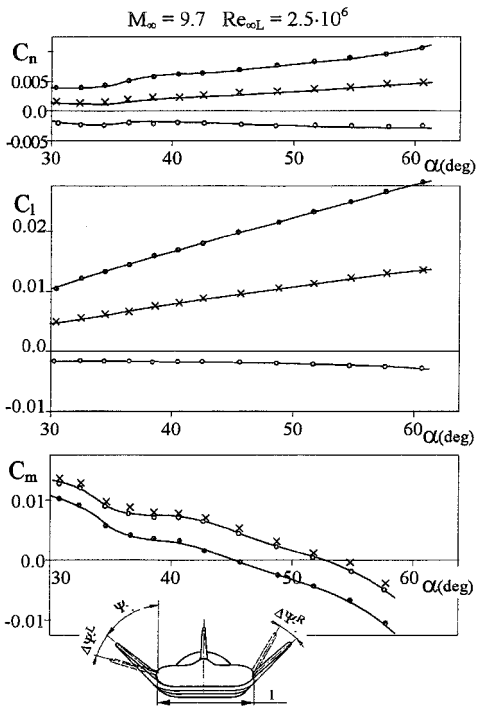

Fig. 9 Yawing-, rolling-, and pitching-moment coefficients of the vehicle model with RAA vs angle of attack at differential wing console deflection: ○, $\Psi^{R/L}$ = 40/40 deg, $\Delta\Psi^{R/L}$ = 0 deg; ×, $\Psi^{R/L}$ = 35/45 deg, $\Delta\Psi^{R/L}$ = ± 5 deg; and ●, $\Psi^{R/L}$ = 30/50 deg, $\Delta\Psi^{R/L}$ = ± 10 deg.

atmospheric trajectory segment, differential deflection of the wing outboards by angles up to $\Delta\Psi^{R/L} = \pm 10$ deg can be accomplished along with the use of gasdynamic control engines. The investigations reveal that the wing outboards effectiveness increases with rising angle of attack (Fig. 9). Additional pitch-up moments caused by differential wing outboards deflections by $\Delta\Psi^{R/L} = \pm 10$ deg cause a decrease in the trim angle of attack by $\Delta\alpha = 7.5$ deg. This change in the vehicle trim angle of attack is within permissible RAA orientation angles ($\alpha_{RAA} = \pm 10$ deg) with respect to the velocity vector (Fig. 9). Similar investigations are carried out in different wind tunnels as applied to the Buran orbiter using its models. These investigations show that because of relatively small sizes of the RAA designed for arrangement on the wing outboard tips their influence on the integral aerodynamic characteristics of this orbiter is very small to manifest itself only over a sufficiently narrow range of transonic velocities.

IV. Heating and Heat Protection of the Remote Antenna Assembly

To investigate heat transfer and heat protection, different approaches are used. As for heat transfer, the main similarity parameters are the Mach and Reynolds numbers, as well as the temperature factor. In the present report heat transfer is investigated at Mach numbers up to $M_\infty = 19.6$, Reynolds numbers based on the pylon diameter up to $Re_{\infty,d} = 0.16 \times 10^5$, and at the ratio of the model surface temperature to the total temperature $T_w/T_t = 0.12$ (respective enthalpy ratio ≈0.1). These values are close to respective parameters at a real flight of Bor-type vehicles. The angle of attack is equal to 55 deg.

To investigate the vehicle heat protection (heat protection of the container nose only is considered in the present report), it is necessary to reproduce full-scale values of the total enthalpy and the stagnation pressure behind the normal shock. Besides, investigations of heat protection demand long-duration tests. Starting with a certain value (of the order of 5), the Mach number exerts a weak influence on the thermal state of the model. In the present report the tests are carried out at the Mach number $M_\infty = 6.5$, total temperature $T_t = 5000$ K (enthalpy $i_t = 14.9$ mJ/kg), and stagnation pressure $P_0 \approx 0.04 \times 10^5$ Pa, which are less than the flight conditions under simulation.

A. Flow Pattern Near the Remote Antenna Assembly

The main peculiarities of the flow pattern are revealed by analysis of schlieren pictures taken during the experiments in the IT-2 wind tunnel at $M_\infty = 19.6$. The additional information is obtained in the T-117 wind tunnel at $M_\infty = 18.7$ using a flow-washed paint applied to the model surface in the form of discrete points.[9]

The flow pattern is shown in Fig. 10. In the lower part of the pylon (Fig. 10b), the bow wave AF, generated ahead of the vehicle body, interacts with the pylon-generated shock CE with the formation of a bridge-like shock system involving almost normal shock AE. The supersonic flow, which passed through the bow wave near point A, decelerates additionally in the oblique shocks AB and BK. Impingement of this high-pressure jet on the pylon surface results in the formation of a zone of increased pressure and heat flux near the point O_1. The second similar pressure and heat flux zone forms at

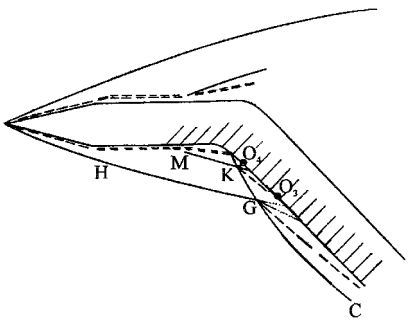

a)

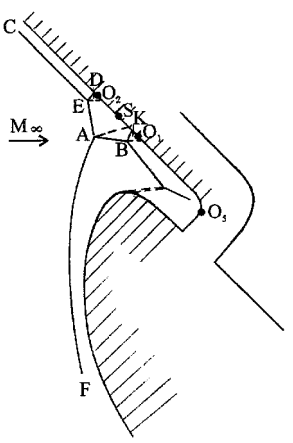

b)

Fig. 10 Flow scheme.

the other end of the bridge-like shock near the point O_2 as a result of successive air compression in the shocks CE and ED. From stagnation point O_1, part of the gas flows toward the container to encounter with the flow going from the point O_2 in the opposite direction; a convergence line S forms between the points O_1 and O_2. The other part of the gas flows from point O_1 downward. The high-pressure jet reaches the pylon base where the stagnation point O_5 forms.

In the upper part of the pylon (Fig. 10a), the container-generated cone shock HG interacts with the shock wave GC generated ahead of the pylon. Because of small angles of inclination of these shocks, a VI-type interference flow, according to the classification suggested by Edney,[10] forms near the point G. In this case a fan of rarefaction waves and a surface of tangential discontinuity emerge from the point G. The rarefaction waves cause a decrease in the heat flux density. However, pressure and heat flux increase considerably above the rarefaction zone (near the point O_3), where the flow is compressed in two oblique shocks GH and GK. The pylon-generated shock KG gives rise to the laminar boundary-layer separation on the container. The separation zone induces the oblique shock MK with a small angle of inclination (6–7 deg). Near the point K, a flow similar to the flow near the point G forms.

B. Aerodynamic Heating

Zones of increased heat transfer are revealed in the T-117 wind tunnel using thermal sensitive paints and ablating materials. Figure 11 exemplifies the picture of the model tested in the T-117 wind tunnel at the following flow parameters: total pressure $P_t = 100 \times 10^5$ Pa, total temperature $T_t = 1800$ K, Mach number $M_\infty = 14$. Replaceable ablating cover plates are mounted on the pylon, which enclose the pylon framework in the front and on the sides. The plates are made of acrylic plastic (polymethylmethacrylate), which decomposes at 500–550 K. A deep cavity O_1 and a smaller cavity O_2 are noted. A sharp rib corresponding to the minimum heat flux forms between them. Regions O_3 and O_4 merge into one region (as in the picture of the model tested using thermal sensitive paints) because of a small distance between regions O_3 and O_4 and of approximately the same heat-transfer level in them. A high-pressure jet, formed in the shock system at the lower bundle of the bridge-like shock, is also responsible for increased heating of the pylon base (at the point O_5). Besides, there occurs a local increase in heat transfer near the pylon base on the leeward vehicle body surface (detected using thermal sensitive paints). In spite of the complicated flow behavior in this region, the heat-transfer pattern at the pylon base is similar to the flow pattern near the cylinder placed on the plate in longitudinal flow.

Most comprehensive and reliable quantitative data on heat transfer are obtained in the IT-2 wind tunnel. The heat flux density is measured by the thin-wall method. The thin wall is made of 0.2-mm-thick stainless-steel foil. Kopel thermocouple wires 0.1 mm in diameter are welded to the internal surface of the foil by spot welding. At the welding spot the wires are flattened to the thickness of 0.03 mm over the length of several millimeters. The thin wall and the thermocouple wire constitute a thermocouple calorimeter gage. The diameter of its active spot is estimated at almost 0.5 mm. The model had 45 thermocouple locations 1.8 mm apart on the leading-edge surface of the pylon and 23 locations 3.3 mm apart on its side surface. The sensitivity of each gauge is determined by calibrating some gauges and introducing individual corrections, which give an account of the real thickness of each gauge (the thickness is measured with an accuracy to about 2.5 μ). The heat flux density is found from the derivative of the gauge signal with respect to time. Investigations show that errors in the heat flux measured by the help of the thin-wall method constitutes about 10 %.

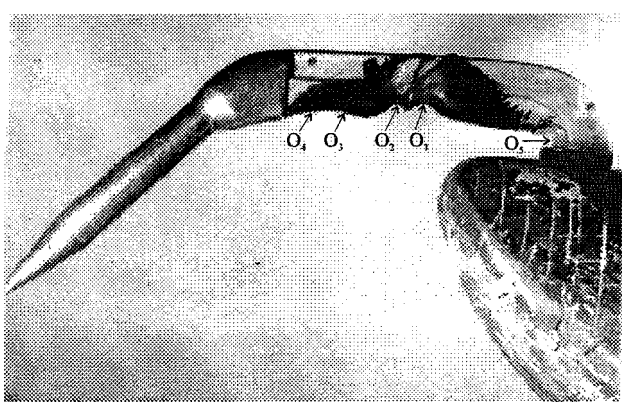

Fig. 11 Model with ablative cover after test.

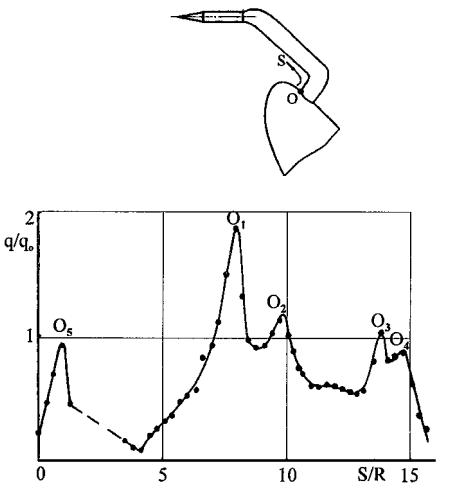

Fig. 12 Relative heat flux distribution.

The experiments in the IT-2 wind tunnel are conducted at $M_\infty = 19.6$ and $Re_{\infty,d} = 0.16 \times 10^5$. The initial pressure in the discharge chamber is 81×10^5 Pa, maximum total pressure is 740×10^5 Pa, initial temperature is 290 K, and maximum temperature is 2400 K. To produce a hypersonic flow, a conical nozzle having the half-angle of 5 deg, throat diameter of 3 mm, and exit diameter of 526 mm is used. The measured heat flux values are related to the calculated heat flux q_0 along the divergence line of the cylinder. It is assumed that the cylinder is in an undisturbed flow, and its diameter is equal to the bluntness diameter of the pylon leading edge ($d = 11.6$ mm). With time the value of q_0 decreases significantly because of the gas pressure and temperature drop. The results given next are obtained at the time moment $\tau = 20$ ms and related to the value of q_0 calculated for the same time moment ($q_0 = 61$ w/cm^2).

Figure 12 shows distribution of the heat flux ratio q/q_0 along the forward pylon generatrix. The coordinate S is also measured along the forward generatrix and related to the pylon bluntness radius $R = 5.8$ mm. The values of q are obtained by averaging the results of 17 experiments. The heat flux distribution on the pylon surface is characterized by a number of maxima and minima corresponding to the flow peculiarities just outlined. The principal maximum refers to the high-pressure jet, which impinges at the stagnation point O_1. Here the heat flux is $(1.8–2.0)q_0$. The greatest scatter in the heat flux values obtained in different experiments ($\pm 15\%$) is recorded at the point O_1. Such scatter is likely to be caused not only by the test condition instability and measurement errors, but also by the flow instability and displacements of the high-pressure jet on the model surface. The second maximum, corresponding to gas deceleration near the point O_2, is much smaller ($q \approx 1.1q_0$). The maximum heat flux values at the pylon base (the point O_5) and in the zone of the container-generated shock impingement (the point O_3) are close to each other: $q \approx 1.0q_0$. The heat flux generated on the container at the end of the separation zone: $q = 0.9q_0$ (the point O_4) is slightly smaller. The heat flux distribution similar to that shown in the figure is obtained for the side generatrix of the pylon. The peak value of the heat flux at the point O_1 is smaller almost by 25% than that on the forward generatrix. For the remaining points the difference is, as a rule, less.

A local maximum of the heat flux is recorded on the upper vehicle body surface immediately at the pylon base. This local maximum is almost $0.6q_0$, which is much smaller than the heat flux maximum at the base of the cylinder placed in a hypersonic flow on a plate in longitudinal flow where it exceeds q_0 greatly.[11] The difference is explained by the fact that in this case the obstacle, i.e., the pylon base, is located in the separated flow region.

The quantitative data on heat transfer are also obtained in the T-117 wind tunnel by using thermal sensitive paints and surface thermocouples at $M_\infty = 18.7$ (description of the method is given in Ref. 9) and by measuring the ablation rate for acrylic plastic at $M_\infty = 14$. In going from the ablation rate to the heat flux value, the effective enthalpy of acrylic plastic is determined by measuring the ablation rate for the frontal surface of a spherically blunted cylinder. Error in the heat flux measured by the help of thermal sensitive points is about 15–20 %. Error of the ablation method is even higher. Taking this in account, one concludes that the heat flux values measured by different methods are in good agreement. Also, the measurements reveal that ablation rate in zone O_1 does not change with time in spite of changes in the pylon configuration. In zones O_2 and O_3–O_4, the ablation rate increases with time. In real conditions, however, when the flight time in the dense atmospheric layers does not exceed 200 s, the expected cavity sizes are small, and a decrease in the pylon sizes may not result in a considerable rise of the heat flux.

The heat flux values measured in the IT-2 wind tunnel are compared with the results of approximate calculations. To do this, the experimental shock inclination values, inferred from the schlieren pictures, and the relationships for plane shocks are used. The calculated maximum relative pressure value on the pylon is $P_{\max}/P_0 \approx 3.5$. Assuming, based on a number of experiments, that the increase in the heat flux in interference zones, when the flow is laminar, is proportional to square root of the pressure ratio, a maximum relative heat flux value $q/q_0 \approx 1.9$ is obtained, which is in agreement with the experimental data at the point O_1. Similarly, at the point O_3 the calculated relative heat flux value $q/q_0 = 1.1$ also agrees with the experimental data.

As a whole, the investigation of heat transfer shows the chosen conditions, namely, at a vehicle angle of attack of $\alpha = 55$ deg and at a pylon inclination angle 45 deg. Relative to the direction of undisturbed flow, the shock wave interference does not result in a catastrophic increase in the heat flux recorded under other conditions (see, e.g., Ref. 10) and does not present insuperable barriers in developing the pylon heat protection.

C. Heat Protection of the Container Nose

The container nose under study is a cone having half-angle of 10 deg and spherical bluntness of $R = 5$ mm. The equilibrium temperature of the bluntness surface during the flight of Bor-type vehicles exceeds the failure temperature of the applied materials. At absence of heat protection, uncontrolled nose melting leads to a rapid increase in the effective bluntness radius and hence in an impermissible growth of the electron concentration in the flow near the container. The only method to retain the nose configuration unchanged is its active heat protection. For reasons of simplicity and reliability, preference is given to the variant with a porous nose and injection of a gaseous coolant through it into the external flow. This method of heat protection is much studied; therefore, it is possible to perform sufficiently justified calculations of the thermal state of the surface to be protected, to estimate needed total coolant mass-flow rates along the flight trajectory, and to determine its required distribution along the coordinate S. Such calculations were carried out using the available information concerning heat transfer at the stagnation point,[12] heat-transfer distribution on blunted cones,[13] influence of gas injection into the laminar boundary layer on heat transfer[14] taking into account gas rarefaction.[15] The length of the protected nose part along the axis is taken to be equal 100 mm, the maximum allowable surface temperature is $T_w = 1000$ K, angle of attack is $\alpha = 0$ deg, and nitrogen is used as a coolant. Permeability must be changed drastically along the coordinate S, especially in the region of matching of the spherical bluntness with the conic surface portion. It follows from the theoretical distribution of the mass-flow rate necessary to provide constant nose temperature. To simplify the problem, the theoretical distribution was approximated by three sections. Within each section the mass-flow rate m is taken to be constant. This mass-flow distribution is shown in Fig. 13 by straight lines in the form of the ratio m/m_0. The porous sample must meet the requirements not only on distribution of the ratio $m(S)/m_0$, but also on m_0 at a specified pressure inside it, i.e., ultimately on the total mass-flow rate. To solve this problem, a special sintering technology is developed for Ni-Cr-alloy powder of porous nose samples 118 mm in length. This technology suggests sintering of separately manufactured spherical section (porosity 60–65%) and conical nose section (porosity 23–25%). Owing to this technology, it became possible to meet both global and local hydraulic characteristics. In all cases air is used for injection. The mass-flow rate was changed at the experiments by controlling pressure inside the models. Correlation of required and actual distributions of the relative mass-flow rate for one of the models is shown on Fig. 13. The data have been obtained by the help of a special probe. The main part of this probe is a differential pressure gauge. It has a tube with a tip pressed during the measurements against the model surface at the test point. It is assumed that the local gas mass-flow rate $m(S)$ is in proportion to $(P_1 - P_2)^{1/2}$, where P_1 and P_2 are pressures respectively in the working and reference chambers of the pressure gauge. The data scatter at fixed S reflects nonuniformity of the mass-flow rate distribution along different model generatrices. It is seen in Fig. 13 that correlation between the required and actual mass-flow rates is good except for the aft part of the model surface.

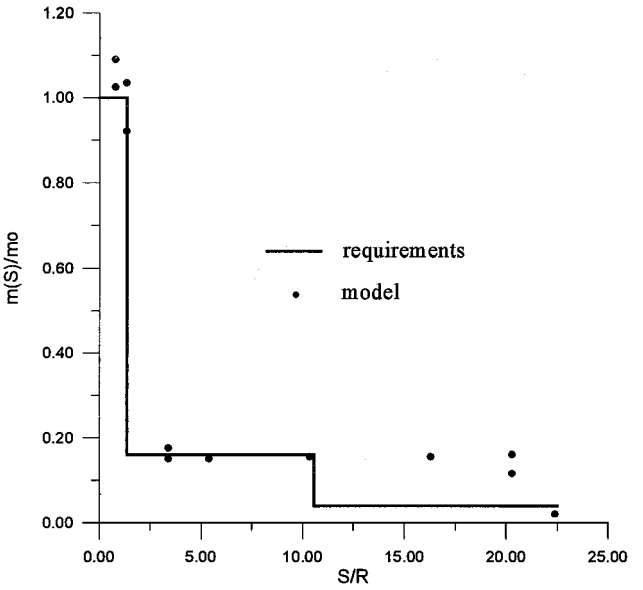

Fig. 13 Relative mass-flow rate distribution.

In the course of the wind-tunnel experiments, the normal operation of the chosen heat protection variant is verified, and the mass-flow rates necessary for heat protection during the long-duration (up to 6 min) experiments were determined. Figure 14 presents the flow pattern without and with injection at the total mass-flow rate $G = 8.7$ g/s. A lamp with the flash duration of 3 micros is used as a light source. The pictures are obtained in the IT-2 wind tunnel at total parameters $P_t = 930 \times 10^5$ Pa, $T_t = 1600$ K, freestream Mach number $M_\infty = 17.9$. The relative mass-flow rate is $\bar{G} \equiv G/\rho_\infty u_\infty F = 0.32$, i.e., somewhat lower than the level $\bar{G} \approx 1$ required for the real flight of the Bor-type vehicle (F is the area of the model middle section). Injection results in a noticeably greater thickness of the boundary layer and in an increase in the effective radius of the nose bluntness. Comparison of the results obtained leads also to the conclusion that the flow is nonstationary at gas injection. The high-temperature tests intended to verify the serviceability of the heat protection method under study have been carried out in the T-122 wind tunnel. A conical nozzle with the exit section of 130 mm has been used. The tests were conducted at $P_t = 5 \times 10^5$ Pa, $T_t = 5000$ K, $M_\infty = 6.5$, and the stagnation pressure $P_0 \approx 0.04 \times 10^5$ Pa. These parameters are chosen in order to approach the flight conditions even though the heat flux at the stagnation point $q_0 \approx 0.3$ kW/cm^2 is still much less than the design maximum value under flight conditions (almost five times).

The injected air is supplied to the model from a high-pressure receiver through a pressure-reducing valve and a throttle orifice. The throttle orifice is necessary to stabilize the mass flow because the drag of the porous model depends greatly on its temperature. The mass-flow rate is determined from the pressure drop rate in the receiver. The measurement error at a mass-flow rate of $G = 1$ g/s

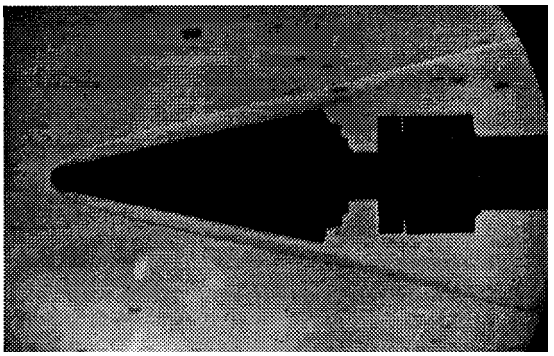

Fig. 14a $M_\infty = 17.9$; $G = 0$ g/s.

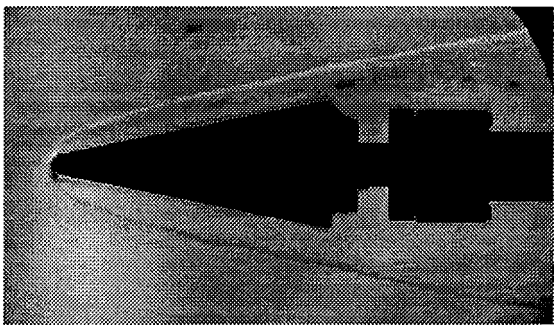

Fig. 14b $M_\infty = 17.9$; $G \approx 8.7$ g/s.

and a maximum test time of 6 min is ±5%. During the tests, an attempt is made to estimate the temperature of the model surface using thermal sensitive paints with melting temperatures of 570, 870, and 1020 K. In all, five models were tested. One of them is manufactured by the conventional technology; therefore, the nose permeability was insufficient. This model was used as a sacrifice with the aim to investigate the failure process at an insufficient mass-flow rate ($G \approx 0.1$ g/s at the initial time moment). The model failure, starting in several seconds after the model was introduced into the flow, is followed by an increased mass-flow rate through the nose with respective increase in the effective bluntness radius, and, as a consequence, further failure slows down. From 5 to 26 tests with the duration from 3 to 6 min were carried out with each remaining four models. In all of the cases heat protection is ensured at $G \geq 0.7$ g/s. In some experiments the model retains unchanged within 3 min at $G \approx 0.5$ g/s, while the surface temperature on the aft model part exceeds 870 K as judged from melting of the thermal sensitive paint. Note that the data obtained are in good agreement with the calculations just considered. According to the calculations, at $G \leq (0.7–0.8)$ g/s the surface temperature increases drastically to attain 1000 K, i.e., the failure temperature, at $G \approx 0.5$ g/s.

Some scatter in minimum mass-flow rates providing heat protection of the test models is basically explained by a nonstationary arc heater operation mode and by changes in the model permeability because of model heating and "bombardment" by particles contained in the flow. Nevertheless, the experiments carried out have confirmed both the capability of realizing the heat protection method under study in principle and the validity of the used estimates of the effectiveness of the coolant injection into the boundary layer. As a conclusion of the experiments, note also that the practical implementation of porous materials in the active heat protection systems necessitates consideration of problems related to the dependence of permeability on contamination and temperature.

V. Conclusions

1) The study shows that acceptable ionization level near the antennas necessary for radio communication with a reentry vehicle can be provided by the help of remote antenna assembly.

2) Experimental study of RAA angles of attack variation and cold gas injection through RAA model nose showed a relatively small impact of these factors on electron number densities in a shock layer.

3) The suggested variant of RAA location in the nose part of the vehicle provides a good aerodynamic vehicle characteristics and essential conditions for radio communication on the plasma trajectory portion.

4) The investigation of heat transfer shows that under chosen conditions, namely, at a vehicle angle of attack of $\alpha = 55$ deg and at a pylon inclination angle 45 deg relative to the undisturbed flow direction, the shock wave interference does not result in a catastrophic increase in the heat flux recorded by many authors under other conditions and does not present insuperable barriers in developing the pylon heat protection.

5) Active heat protection of the container nose using distributed gas injection through porous wall have been investigated in high-temperature flow. The tests approve normal operation of chosen heat protection variant. The experimental value of mass-flow rate providing heat protection is in a good agreement with the calculated one.

6) The gained experience in the investigations involving the developed investigation techniques can be applied to developing the radio communications system for reentry vehicles of other configurations with relatively small bluntness radii of the structure noses and edges.

Acknowledgments

The authors wish to thank L. Yakovleva, Yu. Khodatayev, M. Gladyshev, Yu. Zhilin, S. Chernov, and S. Shilenkov for their assistance.

References

[1] Schexnayder, C. J., "Electron Density Reduction in Re-Entry Plasma due to Nitrogen Atom Removel," *AIAA Journal*, Vol. 8, No. 2, 1970, pp. 375–377.

[2] Rybek, J. P., and Chirchill, R. J., "Progress in Reentry Communication," *IEEE Transactions on Aerospace and Electronic System*, Vol. 7, No. 5, 1971, pp. 879–894.

[3] Gorelov, V. A., Gladyshev, M. K., Kireev, A. Y., Korolev, A. S., Yegorov, I. V., and Byzov, B. N., "Computational and Experimental Investigations of Ionization Near Hypersonic Vehicles," *Journal of Spacecraft and Rockets*, Vol. 33, No. 6, 1996, pp. 800–806.

[4] Czajkovski, E., "Russian Aeronautical Test Facilities," ANSER Center for International Aerospace Cooperation, Arlington, VA, 1994, pp. 1–197.

[5] Park, C., "Review of Chemical-Kinetic Problems of Future NASA Mission, I: Earth Entries," *Journal of Thermophysics and Heat Transfer*, Vol. 7, No. 3, 1993, pp. 385–398.

[6] Gorelov, V. A., Gladyshev, M. K., and Kildusheva, L. A., "Experimental Study of the Electrostatic Wall Probes," *Trudy TsAGI*, No. 2177, 1983, pp. 193–202 (in Russian).

[7] Hayes, D. T., "Electrostatic Probe Measurements of Flow Field Characteristics of a Blunt Body Reentry Vehicle," AIAA Paper 72-694, June 1972.

[8] Gorelov, V. A., Kildusheva, L. A., and Kireev, A. Y., "Ionization Particularities Behind Intensive Shock Waves in Air at Velocities of 8–15 km/s," AIAA Paper 94-2051, June 1994.

[9] Borovoy, V. Ya., Brazhko, V. N., Maikapar, G. I., Skuratov, A. S., and Struminskaya, I. V., "Heat Transfer Peculiarities in Supersonic Flows," *Journal of Aircraft*, Vol. 29, No. 6, 1992, pp. 969–977.

[10] Edney, B., "Anomalous Heat Transfer and Pressure Distributions on Blunt Bodies at Hypersonic Speeds in the Presence of an Impinging Shock," Aeronautical Research Inst. of Sweden, FAA Rept. 115, Stockholm, 1969.

[11] Borovoy, V. Ya., *Gas Flow and Heat Transfer in Zones of Shock Wave-Boundary Layer Interference*, Mashinostroyenie, Moscow, 1983, pp. 1–93 (in Russian).

[12] Fay, J. A., and Riddell, F. R., Theory of Stagnation Point Heat Transfer in Dissociated Air," *Journal of Aeronautical Sciences*, Vol. 25, No. 2, 1958, pp. 73–85.

[13] Bashkin, V. A., and Kolina, N. P., "Calculation of Viscous Drag and Heat Flux on Spherically Blunted Circular Cones in Supersonic Flows," *Trudy TsAGI, Aerodynamic Heating at Hypersonic Flow Velocities*, No. 1106, 1969, pp. 192–267 (in Russian).

[14] Mills, A. F., and Wortman, A., "Two-Dimensional Stagnation Point Flows of Binary Mixtures," *International Journal of Heat and Mass Transfer*, Vol. 15, No. 5, 1972, pp. 969–987.

[15] Provotorov, V. P., and Stepanov, E. A., "Numerical Investigation of a Viscous Shock Layer in the Vicinity of Stagnation Point with Gas Injection," *Uchenye Zapiski TsAGI*, Vol. XVI, No. 4, 1985, pp. 44–53 (in Russian).

I. D. Boyd
Associate Editor